 Human Molecular Genetics, 2002, Vol. 11, No. 11 1251–1262

Targeted disruption of the *Epm2a* gene causes formation of Lafora inclusion bodies, neurodegeneration, ataxia, myoclonus epilepsy and impaired behavioral response in mice

Subramaniam Ganesh[1], Antonio V. Delgado-Escueta[7,†], Toshiro Sakamoto[2], Maria Rosa Avila[5,7], Jesus Machado-Salas[7], Yoshinobu Hoshii[6], Takumi Akagi[3], Hiroshi Gomi[4], Toshimitsu Suzuki[1], Kenji Amano[1], Kishan Lal Agarwala[1], Yuki Hasegawa[3], Dong-Sheng Bai[7], Tokuhiro Ishihara[6], Tsutomu Hashikawa[3], Shigeyoshi Itohara[4], Eain M. Cornford[7], Hiroaki Niki[2] and Kazuhiro Yamakawa[1,*]

[1]Laboratory for Neurogenetics, [2]Laboratory for Neurobiology of Emotion, [3]Laboratory for Neural Architecture and [4]Laboratory for Behavioral Genetics, RIKEN Brain Science Institute, Wako-shi, Saitama, Japan, [5]Departamento de Neurociencias, Universidad Nacional Autónoma de México, Mexico, [6]First Department of Pathology, Yamaguchi University School of Medicine, Yamaguchi, Japan, and [7]Epilepsy Genetics/Genomics Laboratories and Comprehensive Epilepsy Program, UCLA School of Medicine and VA GLAHS West Los Angeles Medical Center, Los Angeles, CA, USA

Received January 16, 2002; Revised and Accepted March 19, 2002

Mutations in the *EPM2A* gene encoding a dual-specificity phosphatase (laforin) cause Lafora disease (LD), a progressive and invariably fatal epilepsy with periodic acid–Schiff-positive (PAS+) cytoplasmic inclusions (Lafora bodies) in the central nervous system. To study the pathology of LD and the functions of laforin, we disrupted the *Epm2a* gene in mice. At two months of age, homozygous null mutants developed widespread degeneration of neurons, most of which occurred in the absence of Lafora bodies. Dying neurons characteristically exhibit swelling in the endoplasmic reticulum, Golgi networks and mitochondria in the absence of apoptotic bodies or fragmentation of DNA. As Lafora bodies become more prominent at 4–12 months, organelles and nuclei are disrupted. The Lafora bodies, present both in neuronal and non-neural tissues, are positive for ubiquitin and advanced glycation end-products only in neurons, suggesting different pathological consequence for Lafora inclusions in neuronal tissues. Neuronal degeneration and Lafora inclusion bodies predate the onset of impaired behavioral responses, ataxia, spontaneous myoclonic seizures and EEG epileptiform activity. Our results suggest that LD is a primary neurodegenerative disorder that may utilize a non-apoptotic mechanism of cell death.

INTRODUCTION

Lafora's progressive myoclonus epilepsy or Lafora disease (LD) is an autosomal recessive, invariably fatal disorder with pathognomonic periodic acid–Schiff-positive (PAS+) intracellular cytoplasmic inclusions (Lafora bodies) in the central nervous system, heart, muscle and liver (1–3). LD starts in early adolescence as stimulus-sensitive grand mal tonic–clonic, absence, visual and myoclonic seizures with electroencephalographic (EEG) 3–6 Hz spike-wave complexes. Rapid neurological deterioration that includes ataxia, dementia, psychosis, dysarthria, amaurosis, mutism, muscle wasting and respiratory failure leads to death between 17 and 30 years of age (2,3). LD, a rare disorder, occurs worldwide but is relatively frequent in the Mediterranean countries of Southern Europe, the Middle East, India, Pakistan and Northern Africa, and in cultures that practice

*To whom correspondence should be addressed at: Laboratory for Neurogenetics, RIKEN Brain Science Institute, 2-1, Hirosawa, Wako-shi, Saitama 351-0198, Japan. Tel: + 81 48 467 9703, Fax: + 81 48 467 7095; Email: yamakawa@brain.riken.go.jp
†Correspondence may also be addressed to: Antonio V. Delgado-Escueta, MD, Epilepsy Genetics/Genomics Laboratories, Comprehensive Epilepsy Program, VA GLAHC Medical Center, 11301 Wilshire Blvd., Los Angeles, CA 90073, USA. Tel: + 1 310 268 3129; Fax: + 1 310 268 4937; Email: escueta@ucla.edu

consanguineous marriages (4–6). LD is caused by mutations in the EPM2A gene encoding a dual-specificity phosphatase named laforin (7–9). Laforin associates with polyribosomes and is expressed ubiquitously (7,9–11). The severity of LD symptoms, its rapid course and death at a young age underlie the important role laforin plays in cell biology.

Because PAS-positive Lafora inclusions are polyglucosan and have been considered to be the hallmark and cause of epilepsy and neurologic deterioration, LD has been traditionally listed under the glycogen storage diseases (2,3). Only a few reports described the degenerative changes in the neuropile (3,12). Perhaps because analysis was restricted to brain and liver biopsy specimens and because a complete postmortem examination was carried out in only a few cases, no study has documented the early neuropathological changes that could define the primary events of the disease. We have generated laforin-deficient mice, and we describe here their primary neuropathologic event, behavioral changes and EEG epileptiform abnormalities.

RESULTS

Generation of Epm2a null mutants

We earlier demonstrated that the fourth exon of the EPM2A gene in humans encodes the dual-specificity phosphatase domain (DSPD) critical for the function of laforin (5). We therefore constructed a targeting vector in which a region of the Epm2a gene encoding the DSPD was replaced by a neomycin-resistance gene cassette (Fig. 1A). This deletion eliminates the coding sequence of the DSPD exon (Fig. 1B). Mice carrying the targeted allele were derived from two independent ES clones. Homozygous offspring for the deletion were viable and were produced in the expected Mendelian genotype ratio of 1 : 2 : 1 (+/+ : +/− : −/−, 115 : 245 : 99) (Fig. 1B). In mice, Epm2a is ubiquitously expressed (10). To define the effects of DSPD exon deletion on Epm2a expression, we compared the RNA extracted from brain and liver tissues of mutants with those of wild-type littermates. No Epm2a mRNA was detected in Epm2a $^{-/-}$ animals when the DSPD region or the coding exons occurring 5′ to the deleted region was used as a probe in northern blot analyses (Fig. 1C). The absence of Epm2a transcripts in homozygous null mutants was further confirmed by reverse transcription–polymerase chain reaction (RT–PCR) analysis (Fig. 1D). Removal of the DSPD exon had therefore prevented expression or maturation of Epm2a transcript, and produced an Epm2a-null mutant.

Null mutants develop Lafora inclusion bodies that are positive for ubiquitin and advanced glycation end-products

We examined the pathology of major organs of Epm2a $^{-/-}$ mice, their heterozygous and wild-type littermates from birth through 1 year of age. Sequential sectioning and staining of brains of Epm2a $^{-/-}$ littermates showed prominent (PAS+) inclusions (Lafora bodies) within neurons throughout the brain (Fig. 2B,D), an observation consistent with findings in LD patients (3). Application of the KM279 antibody, which had been raised against Lafora body extracts from cardiac muscle cells of a patient with LD (13), showed PAS+ inclusions to be antigenetically similar to human Lafora bodies (Fig. 2F,H,J,K). A few small Lafora bodies were observed as early as 2 months after birth. By 4 months, many regions of the brain were extensively loaded with immunoreactive Lafora bodies (Fig. 2J, K). Prominently affected areas include hippocampus, cerebellum, cerebral cortex, thalamus and brain stem (Fig. 2K), which roughly correlate with sites of laforin expression (11). Neuronal Lafora bodies were ubiquitin-positive (Fig. 3A–C), and also reacted with an antibody to advanced glycation end-products (AGEP) (Fig. 3D,E). AGEP are insoluble and non-degradable products that result from the interaction between reducing sugars and long-lived proteins (14–16). Positive reactions in Lafora bodies to antibodies against ubiquitin and AGEP indicate the presence of the polyglucosan protein complex.

Lafora inclusions in non-neuronal tissues

Similarly to LD in human, Lafora bodies were also found in muscle and liver tissues of nine-month-old knockout mice (Fig. 3F,G,I). However, they were not apparent in non-neuronal tissues of four-month old null mutants. Moreover, Lafora bodies of liver and muscle tissues did not react with anti-ubiquitin or anti-AGEP antibody (Fig. 3L,M,N), suggesting different pathological consequence for Lafora inclusions in neuronal tissues. PAS + and immunoreactive Lafora bodies were not detected in the neuronal or nonneuronal tissues of heterozygous and wild-type littermates (Fig. 3F,G,J).

Ultrastructural analysis: neuronal cell death in homozygous null mutants

To further understand the mechanism of cell death at 2 months and the pathological consequences of Lafora bodies in homozygous null mutants, we studied the fine structure of their neuropile (Fig. 4). Ultrastructural analysis in knockout mice brains revealed isolated or full rows of cerebellar Purkinje cells, hippocampal pyramidal and granular cells, and cerebral cortical pyramidal cells showing unequivocal features of somatic degeneration as early as 2 months of age (Fig. 4A–H). Distorted and shrunken cytoplasmic and nuclear membranes characterized these dark neurons (Fig. 4A). Most organelles in such cells showed disruption of their normal distribution, and their essential morphological features were lost. Dark mitochondria, dilated cisterni of endoplasmic reticulum, and displaced and collapsed Golgi apparatus were prominent and consistently observed changes (Fig. 4B). Neuronal processes and their organelles also showed disruption of structures (Fig. 4C–F). Longitudinal or transverse dendritic sections showed atrophic and distorted spines that were homogenously hyperdense. Some were shrunken and their organelles showed degenerative changes (Fig. 4C), whereas others were either hyperdense or vacuolated (Fig. 4D). Frequently, a normal synaptic bouton was impinging upon these degenerated dendrites (or upon their spines). Transverse sections of axons showed distortions and disruptions of myelin sheaths, with abnormal separation of lamellae, and a central, dense body with degenerated organelles (Fig. 4E). Axoplasm appeared watery and vacuoles formed. Mitochondrial cristae were no longer observed, and were

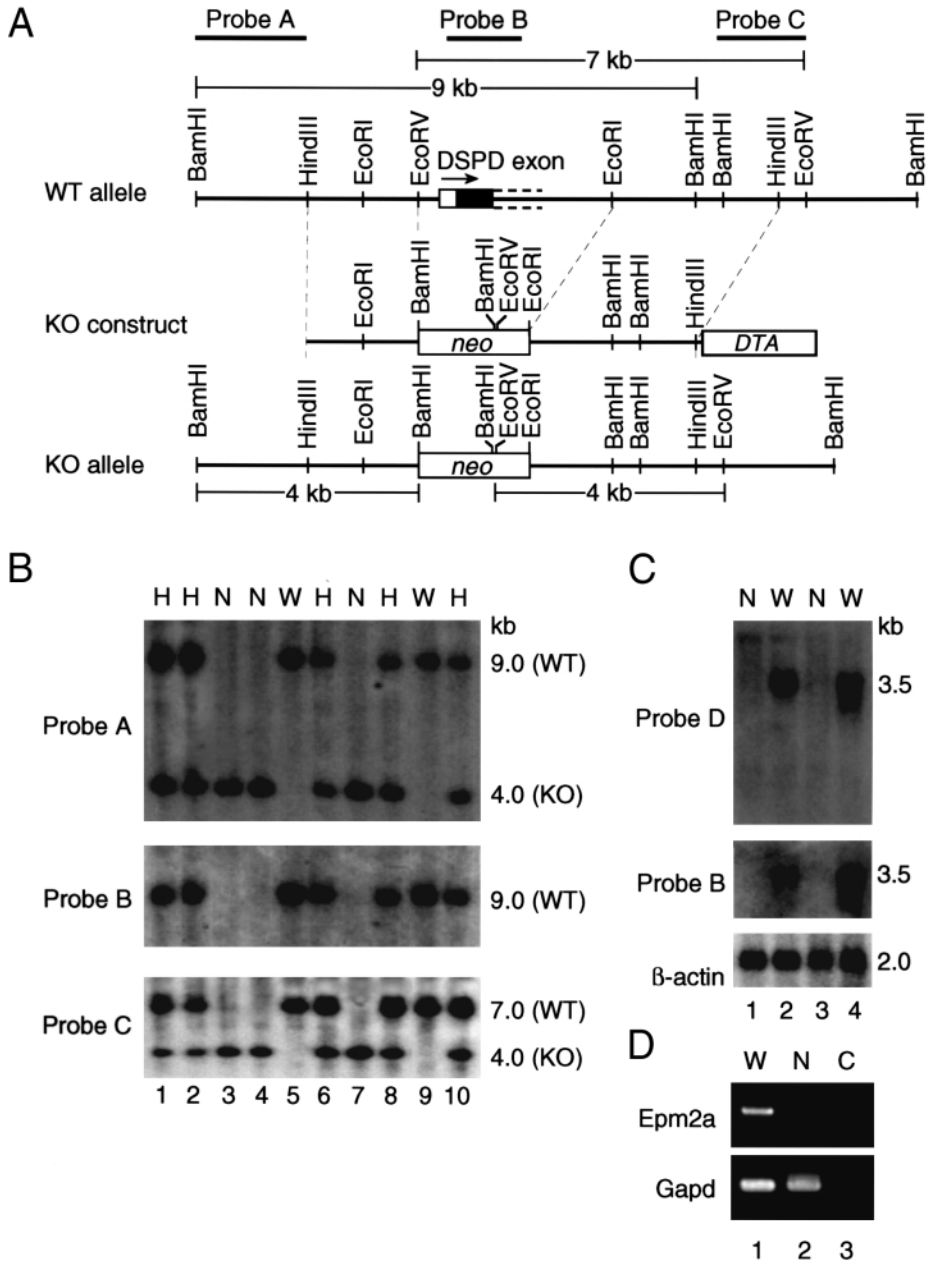

Figure 1. Generation of laforin-deficient mice (Epm2a $^{-/-}$). (A) Schematic diagram of the Epm2a genomic clone B6LDM8 (top), the targeting construct (middle), and the targeted Epm2a allele (bottom). The coding (white box) and non-coding (blackened box) regions of the exon encoding the DSP domain are shown. The cDNA clones isolated for the murine Epm2a gene were partial for presumptive 5′- and 3′-untranslated regions (UTR) (10); therefore the 3′ end of the DSPD exon could not be defined (shown in dotted lines). Relative positions of the 5′ external probe (Probe A), and two internal probes (Probes B and C) used to detect the targeted allele are shown on the top. The predicted size of the wild-type and targeted alleles that Probes A and C would detect in BamHI and EcoRV digests respectively are also shown. Probe B is an 800 bp cDNA insert of the clone LDM5 (10). (B) Southern analysis of BamHI- (for Probes A and B) and EcoRV (Probe C)-digested genomic DNA from mouse-tail cuts. Lanes 3–10 are F_2 littermates born to F_1 heterozygotes (lanes 1 and 2). Probes A and C identified expected size fragments of wild-type (WT) and targeted (KO) alleles, and Probe B confirmed the deletion of DSP exon in the homozygous null mutants. Lanes 1, 2, 6, 8 and 10 are heterozygotes (H), lanes 3, 4 and 7 are homozygous null mutants (N) and lanes 5 and 9 are wild-type samples (W). No hybridization signal was detected when the DTA cassette was used as a probe (data not shown). (C) Northern blot analysis of Epm2a. Poly(A) RNA (6 µg) extracted from brain (lanes 1 and 2) and liver (lanes 3 and 4) tissues of wild-type (W) and mutant (N) animals were probed with a 618 bp Epm2a cDNA fragment (Probe D) representing the 5′-UTR (66 bases) and coding regions of exons 1, 2 and 3 (551 bases) but not the DSPD exon (exon 4). The 3.5 kb Epm2a transcript is absent in the Epm2a $^{-/-}$ mouse. An Identical result was obtained when the blot was hybridized with Probe B, suggesting that removal of the DSPD exon affected the expression or maturation of the Epm2a transcript. A β-actin probe was hybridized to the same blot to assess the approximate quantity of RNA loaded in each lane (lower panel). (D) RT–PCR analysis for Emp2a expression in knockout mice. A forward primer annealing to exon 3 (5′-aatatctggctgggtagctgcc-3′) and a reverse primer annealing to exon 4 (5′-aggttccttactaaggcagctagacg-3′) were designed to amplify a 554 bp fragment from the Epm2a cDNA. The RT–PCR analysis, performed on cDNAs derived from total brain RNA, resulted in amplification of the expected size fragment in the wild-type (W) but not in the homozygous null mutant (N) sample, confirming the absence of Epm2a transcripts in the knockout mice. Lane 3 refers to the reaction (C) without a template. Control amplification for the glyceraldehydes 3-phosphate dehydrogenase gene (Gapd) confirms the quality of the cDNA made.

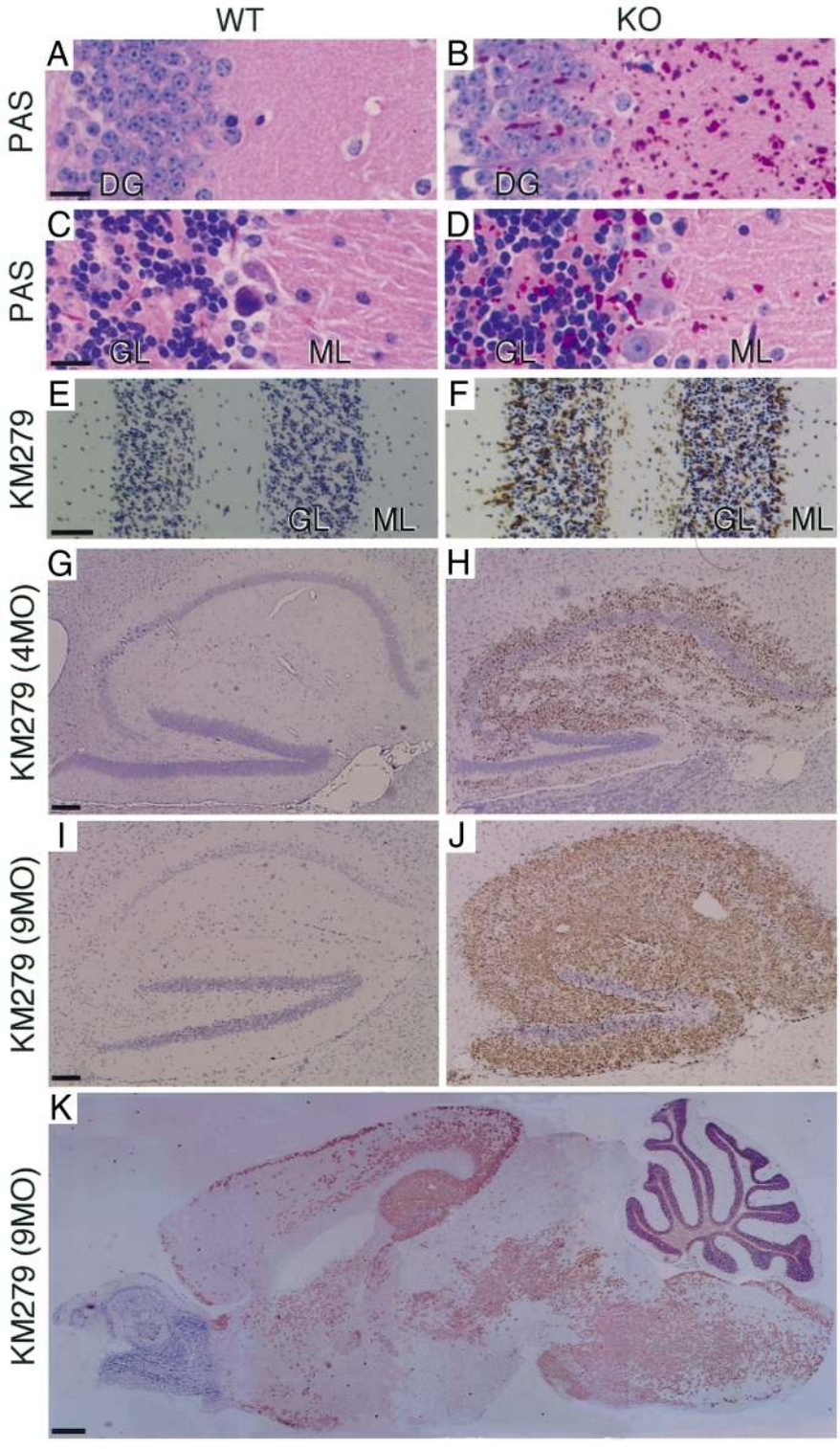

Figure 2. Histochemical localization of Lafora inclusions in Epm2a $^{-/-}$ mice brains. Periodic acid-Schiff-positive (PAS +) granules are shown in the hippocampal (B) and cerebellar (D) regions of the 9-month-old mutant mice (KO). PAS + granules were observed in the granule cell soma and process of the dentate gyrus (B) and predominantly in the granule cell layer of the cerebellum (D). PAS + granules were not seen in the wild-type littermates (WT) (A, C). (E–K) Immunostaining of Lafora bodies with biotinylated monoclonal antibody KM279. Cerebellar region of a 9-month-old mutant mouse showing predominant immunoreactivity for Lafora bodies in the granule cell layer as observed by the PAS staining (F). KM279 immunoreactivity in the hippocampi of a 4-month-old (4MO) (H) and a 9-month-old (9MO) (J) knockout mouse. Accumulation of immunoreactive granules increased with age in most of the regions of brain (K) but not in wild-type littermates (G, I). Sections (E–K) were counterstained with hematoxylin. DG, dentate gyrus; GL, granule cell layer; ML, molecular cell layer. Scale bar = 10 μm (A–D), 50 μm (E, F), 100 μm (G–J) and 500 μm (K).

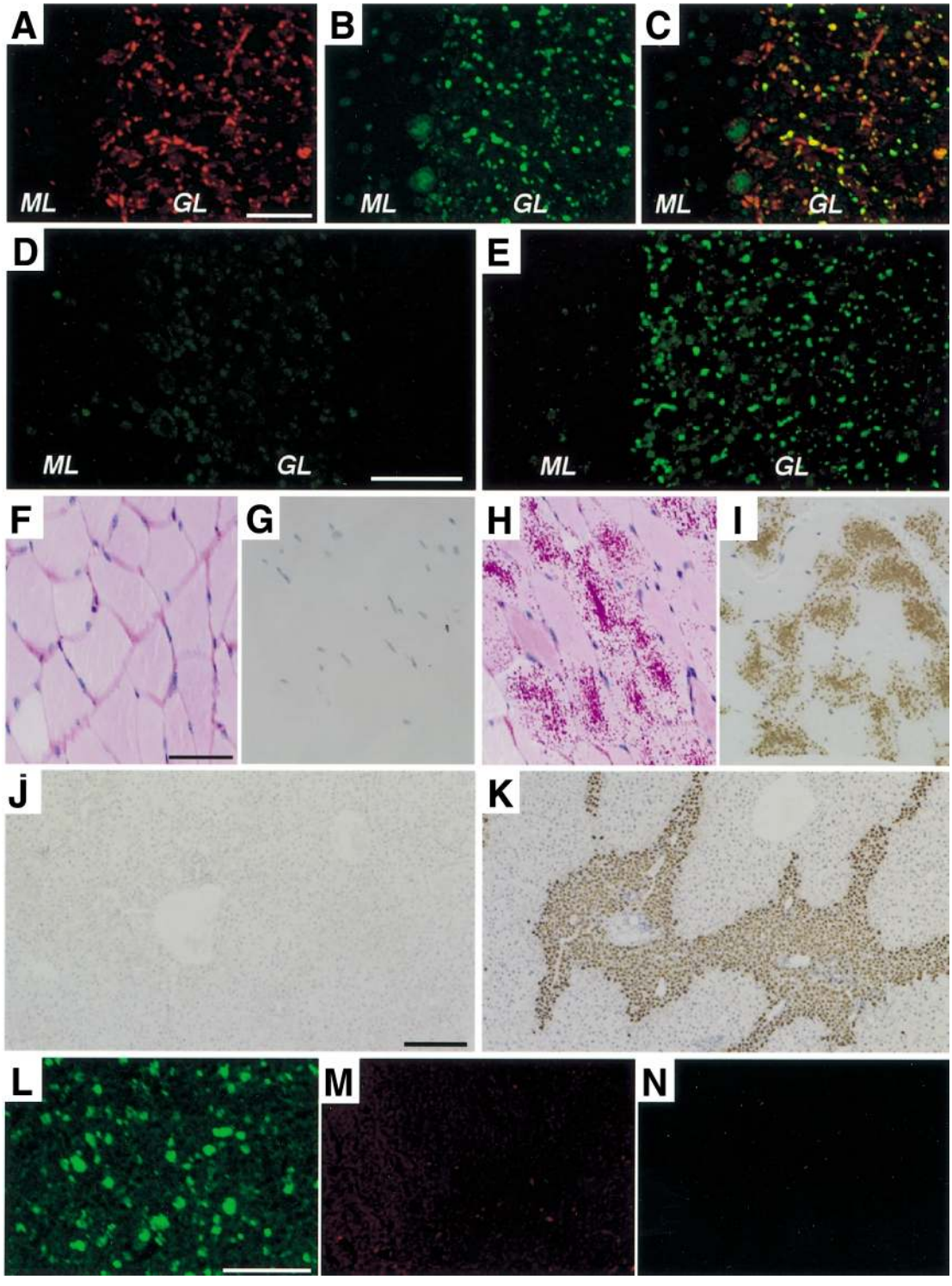

Figure 3. Lafora bodies in neuronal and non-neuronal tissues. Neuronal Lafora bodies are ubiquitin-positive. Cerebellar section of a 9-month-old null mutant's brain was double-stained with the anti-Lafora body antibody KM279 (mouse monoclonal; red) (A) and anti-ubiquitin antibody (rabbit polyclonal; green) (B) (C) co-localization (yellow) of staining for Lafora bodies (red) with ubiquitin (green) in cerebellar neurons. Cerebellar sections of 9-month-old wild-type (D) and null mutant (E) littermates were immunostained with anti-AGEP antibody. A double staining with KM279 could not be performed, since both were mouse monoclonal antibodies. However, from its identical staining profile to KM279 in serial sections (not shown) and absence of any signal from the wild-type brain section (D), it could be inferred that anti-AGEP specifically reacted to Lafora inclusions. No signal was observed when primary antibody was omitted for immunostaining (data not shown). PAS (F, H) and KM279 immunostaining (G, I, J, K) for muscle (F–I) and liver (J, K) tissues of 9-month-old wild-type (F, G, J) and mutant (H, I, K) littermates. Liver tissue section from a homozygous null mutant was double-stained using KM279 antibody (L) and ant-ubiquitin antibody (M). A serial section of the same tissue was also stained for the anti-AGEP antibody (N). Note the absence of any signal for the anti-ubiquitin and anti-AGEP antibodies. GL, granule cell layer; ML, molecular cell layer. Scale bar = 50 μm (A–E), 500 μm (D–K), 25 μm (L–N).

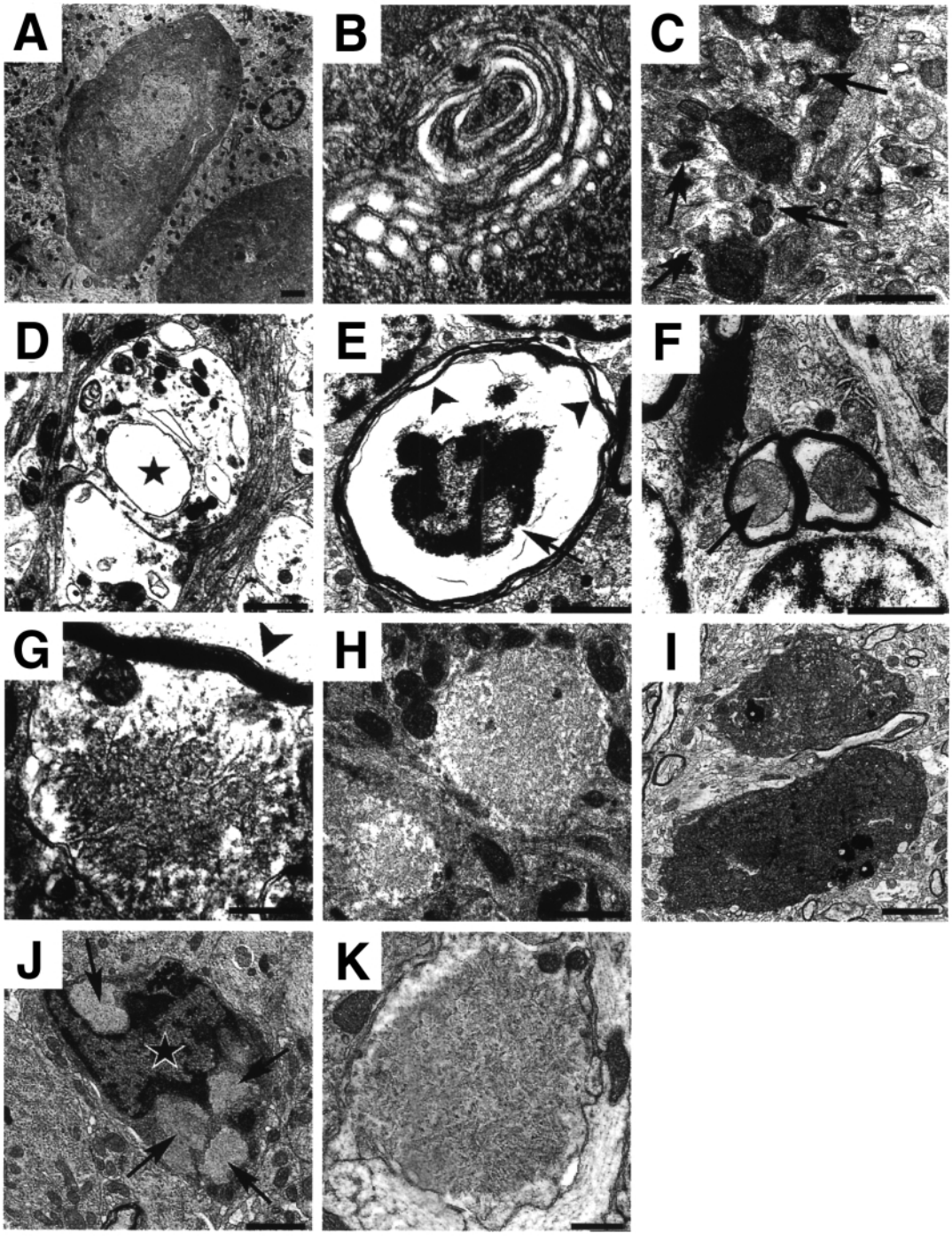

Figure 4. Ultramicroscopical changes observed in nerve cells from Epm2a $^{-/-}$ mice. Images (A–H) are from 2-month-old and those (I–K) are from 9-month-old mice. (A) Two Purkinje neurons from cerebellum display signs of degeneration. Dark and shrunken cytoplasm, with dilated cisterni, hyperdense mitochondria, lipofuscin granules and a distorted and invaginated nucleus characterize these neurons. A cerebellar granule contains a few dark bodies together with normal organelles. (B) An enlargement of the Golgi apparatus zone from one of these dark neurons illustrates prominent dilation of cisterni. (C) Low-magnification view from the cerebellar cortex of a null mouse depicting three dark neurites surrounded by a normal neuropile. They correspond to transverse sections of secondary or tertiary dendrites, and have lost volume and become hyperdense. Remnants of the synaptic complex still can be identified in one of its spines and on several other degenerated gemmules (arrows). (D) Dendrites show several degrees of degeneration. In this case, early vacuolization (star) and dark-body formation can be seen. Attached to this dendrite there is a watery, degenerated neurite – perhaps a non-functional terminal bouton. (E) The axonal processes are frequently altered. This transverse section of a myelinated axon displays a distorted myelin sheath (arrowheads), a watery axoplasm and a central dark body with a granular and a dense component (arrow). (F) Two swollen mitochondria (arrows), without recognizable cristae are seen inside of two small axons. (G) A cerebellar neurite depicting an early formation of Lafora body. The Arrowhead indicates the myelin sheath. (H) High magnification of two intracytoplasmic Lafora bodies in a Purkinje cell. Notice its globular aspect and its fine, microfibrillar array. (I) Two cerebral cortex neurons displaying advanced degenerative changes. (J) A hippocampal pyramidal neuron loaded with Lafora bodies (arrows), which impinge and distort the nucleus (asterisk). (K) A higher magnification of a Lafora body in the perikaryon of a Purkinje cell. Scale bar = 1 μm (A), 0.5 μm (B), 1 μm (C), 0.5 μm (D), 1 μm (E), 1 μm (F), 0.5 μm (G), 1 μm (H), 2 μm (I), 2 μm (J), 0.5 μm (K).

replaced by fine granular material (Fig. 4F). Degenerating neurons were observed in EM preparations of 2-, 3-, 9- and 10-month-old knockout mice. Most degenerating neurons did not show Lafora inclusion bodies.

There was no fragmentation or 'blebbing' of either nucleus or cytoplasm of degenerating cells. Repeated attempts to identify DNA fragmentation by in situ labeling with terminal deoxynucleotidyl transferase(TdT)-mediated dUTP nick-end labeling (TUNEL) method failed to reveal a significant increase in the number of positive cells in the null mutant's brains when compared with wild-type and heterozygote littermates.

Ultrastructurally, Lafora inclusions in the knockout mice were very similar, if not identical, to electron-microscopic descriptions of Lafora bodies in humans (3). These inclusion bodies were formed by small, fragmented fibrillar material surrounded by abundant fine, punctiform particles that resembled ribosomes (Fig. 4G,H,J,K). Most inclusion bodies were relatively hypodense, but occasionally their density appeared darker. There was no limiting membrane surrounding these Lafora bodies. The appearance was very similar in experimental animals from all ages, as shown in 2-month-old (Fig. 4H) and 9-month-old null (Fig. 4K) mutants. In general, inclusion bodies showed variable sizes that increased in dimension with age. Figure 4G displays the beginning formation of a small Lafora body, within a neurite. Figure 4H is a high magnification of two intracytoplasmic Lafora bodies that barely displace mitochondria and other organelles. In contrast, in 9-month-old animals, the neuronal cytoplasm can be completely filled with larger Lafora inclusions that often displace the nucleus and organelles (Fig. 4J).

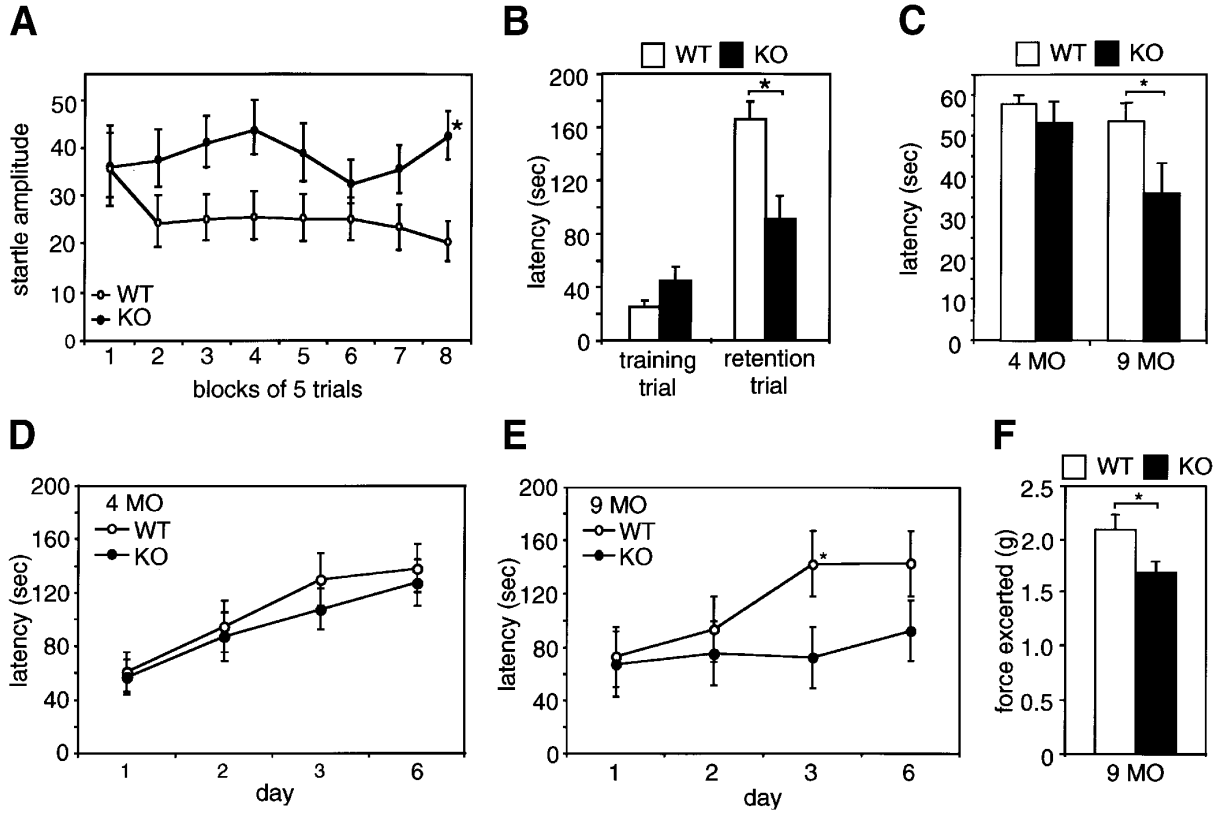

Figure 5. A summary of behavioral analyses for Epm2a $^{-/-}$ mutant mice. (A) Startle response test: course of acoustic startle amplitude during 110 dB 40-pulse trails for 4-month-old Epm2a $^{-/-}$ (KO) and wild-type (WT) littermates. Data are shown as mean (± SEM) acoustic startle reflex amplitude in blocks of five trials (n = 8, each genotype). Mutant mice show significant difference in the startle amplitude for the last five pulse trails (2-way ANOVA test, $P < 0.0223$). Overall significant difference between the two genotypes, $P < 0.0131$. (B) Passive avoidance test for 4-month-old littermates. Plotted is the latency (± SEM) to enter the dark chamber during the training trial and the retention trial. The retention trial was conducted 24 hours following training. KO mice were significantly impaired in passive avoidance retention test (Mann–Whitney U-test, $P < 0.0062$; n = 22, each genotype). Comparison of the average performance of WT and Epm2a mutant mice (KO) on wire-hanging (C) and rotorod (D, E) experiments performed on 4-month-old (4MO) and 9-month-old (9MO) animals. The mean latency to stay on the wire-hang task is shown in (C) (n = 12, each genotype). The 9MO mutant mice (KO) fell off the screen in a significantly shorter time than the wild-type littermates (WT) (Mann-Whitney U-test, $P < 0.0487$). There was no significant difference in the performance of the 4-month-old (4MO) age group. For the rotarod test (D, E), each mouse was tested for three trials on succeeding days and the fourth trial was done on day 6, after a gap of 2-day rest. Error bars correspond to SEM (n = 12, each genotype). Overall, a significant difference in the latency to stay on the rotarod was obtained between the wild-type and mutant littermates of the 9-month age (9MO) group (2-way ANOVA test, $P < 0.0348$). The mean latency on day 3 in the 9MO age group was significantly different between the two genotypes ($P < 0.0391$). The mean difference continued to day 6; however, it did not attain statistical significance. There was no significant difference ($P > 0.5$) between the two genotypes of the 4-month age group (4MO) in their performance on rotarod. (F) Quantitative measurement of muscle strength in mutant mice using a dynamometer. The values are the mean average of force exerted per gram body weight (n = 15, each genotype). The mutant mice (KO) performed significantly worse than the wild-type (WT) littermates (1-way ANOVA test, $P < 0.0302$). There was no significant difference in body weight among the genotypes.

Epm2a null mutants show impaired behavioral response and progressive ataxia

In spite of the appearance of a few small Lafora inclusion bodies and signs of neurodegeneration on electron microscopy at 2 months, the Epm2a $^{-/-}$ mice appeared to grow and develop normally during the first 3 months. At 4 months, the magnitude of acoustic startle reflex in Epm2a $^{-/-}$ mice in response to a stimulus of standard intensity remained high throughout the whole test session (Fig. 5A). This suggests a deficit in habituation and/or enhanced excitability/diminished inhibition in central nervous system pathways. In the passive avoidance task, null mutants showed a deficit in retention (Fig. 5B). Taken together, these results indicate impaired behavioral response in 4-month-old null mutants due to inactivation of the Epm2a gene.

At 9 months of age, muscular weakness and ataxia were grossly evident in null mutants. Rotarod and wire-hanging tasks showed significantly impaired motor coordination, balance and grip strength in 9-month-old Epm2a $^{-/-}$ mice when compared with wild-type littermates (Fig. 5C,D,E). Mean neuromuscular strength and endurance force exerted in a dynamometer by 9-month-old mutant mice were significantly less than that of wild-type littermates (Fig. 5F).

Myoclonic seizures and EEG epileptiform activity in null mutants

Nine-month-old Epm2a mutants also developed spontaneous myoclonic seizures with an approximately 80% penetrance (in 24 out of 30 animals observed). Ear and head spasms and shoulder jerks or minor shaking of the torso followed by an upward motion of the head at times forced the animal forward. Each episode lasted for a few seconds and usually consisted of one or two jerks. Frequency of seizures was measured by an automated seizure detection system (17). Several spontaneous seizures were observed during the animals' dark and light cycles, but the frequency was almost doubled during active (dark) periods. Scalp EEG and cortical electrography in mutant mice revealed frequent single spikes, repetitive spikes and sharp waves as well as spike and slow-wave formations that appeared synchronously

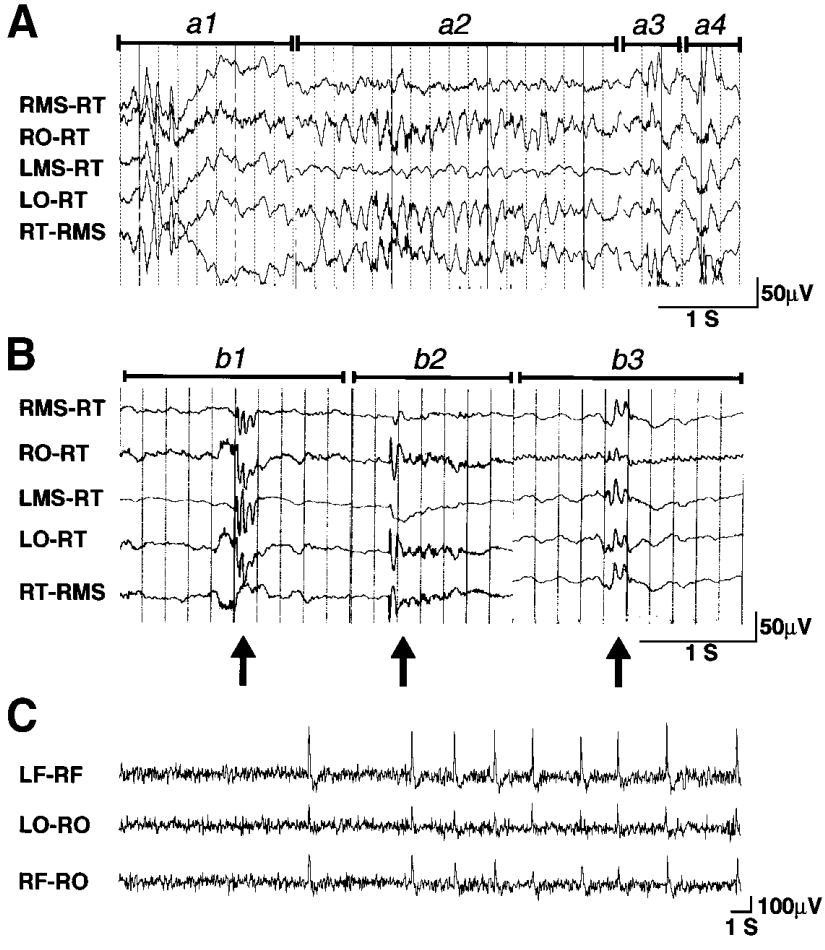

Figure 6. EEG and ECoG recordings in Epm2a $^{-/-}$ mice. (A) The EEG in null mutants recorded during sleep: (a1) 100 mV sharp waves that burst in clusters of three discharges; (a2) in runs of 3 seconds or more consisting of 5–7 Hz repetitive sharp waves; (a3) random spikes and sharp waves, and (a4) irregular spike and slow-wave formations. (B) Simultaneous recording of myoclonic seizure (arrows) and corresponding EEG epileptic discharges (polyspikes). Three independent episodes (b1, b2 and b3) are shown. (C) High amplitude spikes firing in both hemispheres in synchrony were observed in ECoG of null mutant. RT, right temporal region; RMS, right motor sensory area; LMS, left motor sensory area; LO, left occipital area; RO, right occipital area; LF, left frontal area; RF, right frontal area.

or asynchronously in both cerebral hemispheres during awake and sleep periods (Fig. 6). Diffuse polyspikes followed by slow waves were also evident in the EEG during spontaneous myoclonic jerks (Fig. 6B). Awake cortical electrography also showed a reduction in the background frequency of the brain waves in the 9-month-old knockout mice (data not shown).

DISCUSSION

We have established a mouse model for LD through targeted disruption of the Epm2a gene. The phenotype resulting from the loss of the Epm2a gene in mice is comparable to the phenotype of human LD resulting from the same genetic defect. The Epm2a $^{-/-}$ mice are developmentally normal and fertile, but developed behavioral abnormalities at 4 months and signs of ataxia, and myoclonus epilepsy at 9 months of age. At 2 months of age, homozygous null mutants developed widespread degeneration of neurons, most of which occurred in the presence of only a few small Lafora inclusions. Mitochondrial, endoplasmic reticulum and Golgi apparatus swelling with lysis of cell membranes led to cell death. As Lafora bodies became more prominent at 4–12 months, organelles and nuclei were disrupted. Neuronal cell death and Lafora inclusion bodies predate impaired behavioral responses, ataxia, myoclonic seizures and EEG epileptiform activity. Our results suggest that LD is primarily a neurodegenerative disorder and provide evidence for laforin's critical role in neuronal survival.

Laforin deficiency in both humans and mice results in the formation of Lafora inclusions, progressive ataxia and myoclonic seizure. However, the mutant mice only developed spike and slow-wave formations, but not the regular and well-formed EEG difuse 3–6 Hz spike-wave complexes. Clinical absences or grand mal tonic–clonic seizures, which are almost invariably observed in LD patients, also did not develop in 1-year old mice. This suggests that additional factors (environmental or genetic) contribute to the appearance of grand mal and absence seizures in humans. Alternatively, such factors could reflect differences in the organization/functions of cortico–reticular–cortical pathways between mice and humans. As the null mutants analyzed in the present study were up to 1 year old, it is also possible that they will develop other elements of LD as they age. Such an extended study may also resolve the difference, if any, in the lifespan of the null mutants – an anticipated phenotype, but not seen in our 1-year-old mice colony.

Previous neuropathological studies for LD in humans have been limited to gross anatomical descriptions of autopsy results and did not characterize in detail the structural abnormalities. Moreover, these results in humans were complicated by chronic diphenylhydantoin treatment, which is known to produce cerebellar degeneration. Thus the contributions of chronic diphenylhydantoin treatment to the neuropathology found in LD were never resolved in humans. Our finding that the disease phenotype in knockout mice is associated with widespread neuronal degeneration earlier than had been reported in human LD provides new clues to the evolution and pathogenesis of LD. Neuronal cell death was found in all stages of null mutants analyzed (2- to 12-month old animals). However, a rigorous quantitative analysis for different age groups is necessary to understand the spatial and temporal difference in the number and distribution of degenerating neurons in null mutants' brains. Degenerating neurons exhibit cellular darkening, nuclear and cytoplasmic condensation, swelling of subcellular organelles, and structural abnormalities in the neuronal processes. However, the defining characteristics of apoptosis – the fragmentation or blebbing of both cytoplasm and nucleus – were not found in the degenerating neurons. Similarly, the absence of TUNEL-positive cells in null mutants' brains suggests that within degenerating neurons there is no DNA fragmentation, a prominent feature of apoptotic cells, and that cell death occurs without activation of apoptosis. It is noteworthy that morphologically very similar forms of cell death have been described previously in neural degeneration in Huntington disease patients and in Huntington model mouse (18). Further, it has been suggested that such forms of neuronal cell death may define a novel process that is morphologically and biochemically distinct from apoptosis (18). It is surprising that the loss of function of a normally ubiquitous protein, laforin, cause selective neuronal loss. One possibility is that laforin has a neuron-specific substrate whose activation/inactivation is critical for neuronal survival. The detection of cell death in laforin-deficient mice supports the interpretation that at least some of the symptoms of LD are initiated by neuronal death.

In addition to the PAS reactivity, biochemical studies in humans have indicated that Lafora bodies are principally composed of polysaccharides (19,20). A recent report demonstrates that laforin contains a functional carbohydrate-binding domain at its N terminus that targets laforin to glycogen (21). This raises an interestingly possibility, supported by recent studies by Raben et al. (22). By targeting the glycogen complex in vivo, laforin as a dual-specificity phosphatase may regulate proteins, such as glycogen synthase, that are involved in glycogen synthesis. Loss of function of a mutated laforin would lead to an overdrive in glycogen synthesis and the accumulation of polyglucosan as Lafora bodies. Alternatively, laforin may mediate the disposition of Lafora bodies by directly binding to these inclusions. Polyglucosan bodies are known to be produced normally in neuronal cells and cleared via axons into the cerebrospinal fluid (23). Thus, laforin may be involved in the inter- and intracellular migration of polyglucosan, and its loss of function would result in polyglucosan accumulation as Lafora bodies. Our observations on PAS+ inclusions increasing in dimension with age in laforin-deficient mice are consistent with both propositions. Our knockout mouse model provides a valid model to test both of these hypotheses.

Are Lafora bodies toxic to neuronal cells? Since the majority of degenerating neurons do not contain Lafora bodies and not all cells that contain Lafora inclusions degenerate, the formation of Lafora bodies may not necessarily lead to neuronal cell death. However, a causative role for Lafora inclusion in neuronal dysfunction cannot be excluded. Inclusions harboring ubiquitin and/or AGEP modified proteins have been implicated in the pathogenesis of a number of degenerative diseases (24–30). Lafora inclusions may thus induce neuronal stress and neurotoxicity due to a diminished ubiquitin proteolytic system (27,30,31) and/or by generation of reactive oxygen species

through an interaction between AGEP and RAGE (receptor for advanced glycation end-products) (32–35). Importantly, the early onset of both neurodegeneration and Lafora inclusion in Epm2a-knockout mice predates behavioral abnormalities, ataxia and epileptic myoclonias by many months. Any attempt to treat LD in humans must therefore start at the presymptomatic stages of the disease in early childhood. The Epm2a $^{-/-}$ mouse model of human LD, with its progressive and profound neurologic disturbances and pathology, should be critical in developing treatment such as gene therapy.

METHODS

Generation of Epm2a-deficient mice

We deleted the dual-specificity phosphatase domain (DSPD) coding region of the Epm2a gene (Fig. 1A). A 15 kb genomic clone B6LDM8 identified in a previous study (7) was used to make a targeting construct. A 2.0 kb HindIII–EcoRV fragment and a 3.0 kb EcoRI–HindIII fragment of the B6LDM8 clone were subcloned respectively into the HindIII and SmaI sites and EcoRI–HindIII sites of the plasmid vector pBluescript IISK+ (Stratagene Inc., La Jolla, CA). Subsequently, the 2.0 kb HindIII–EcoRV fragment was excised by HindIII and BamHI digestion and cloned into HindIII and BamHI sites of a targeting vector, generating the 5′ arm of the construct (Fig. 1A). The 3′ arm was generated by inserting the 3.0 kb EcoRI–HindIII fragment into the EcoRI and HindIII sites, thus creating the neomycin phosphotransferease (neo) targeting cassette (Fig. 1A). Another negative-selection cassette (DTA), which encodes the diphtheria toxin A-fragment under the control of the HSV-tk (herpes simplex virus thymidine kinase gene) promoter, was included in the targeting construct to allow enrichment for the correctly targeted embryonic stem (ES) cell clones.

The targeting vector linearized with NotI was electroporated into approximately 5×10^7 E14 ES cells with a Gene-Pulser (Bio-Rad Laboratories, Hercules, CA) at 3 μF and 800 V. Transfected cells were plated on neomycin-resistant, mitomycin C-treated mouse embryonic feeder cells (MEF) in a 10 cm dish. One day after plating, positive selection was performed in the presence of Geneticin (G418; 125 μg/ml). Resistant clones were picked at day 9 and subsequently expanded into 24-well plates preseeded with MEF. BamHI-digested genomic DNA from individual clones was analyzed by Southern blot with a 1.5 kb probe derived from the genomic sequence immediately upstream of the targeting vector (Probe A; Fig. 1A). The probe was generated by subcloning the 1.5 kb BamHI–HindIII fragment into a pBluescript II SK+ vector. Positive clones were further confirmed by hybridizing the EcoRV-digested genomic DNA to a 3-end probe (Probe C, ∼1.5 kb BamHI–EcoRV fragment; Fig. 1A). Approximately 15 ES cells from each of the two targeted clones (S31 and S128) were injected into C57BL/6J blastocysts. An average of 15 injected blastocysts were transferred into pseudopregnant female recipient ICR mice. Both ES clones produced several chimeras with greater than 50% agouti coat color. Eight (four for each clone) male chimeras were bred to C57BL/6J females to allow for the detection of germline transmission by the agouti coat color marker. Thirty-eight percent of the agouti offspring (92 of 237) were positive for the insertion, as determined by Southern blot analysis. Heterozygous mice were crossed to generate animals homozygous for the insertion. All observations reported here were made using the F_2 generation, mixed C57BL/6 and 129Svj genetic background animals from lines derived from ES clones S31 and S128. While histological and EEG/EcoG examinations were done on both lines, behavioral analysis was restricted to a single line (S31 only).

Expression analysis

Liver and brain tissues were dissected from 2-month-old mice, and RNA was extracted as described previously (11). Six micrograms of poly(A) RNA was loaded per lane on 1% agarose formaldehyde gel, and the size-separated RNA was transferred to a nylon membrane (Biodyne; Pall Bio Support, East Hills, NY). For hybridization, DNA probes were labeled with [α-^{32}P]dCTP and hybridized overnight in ExpressHyb hybridization solution (Clontech, Palo Alto, CA) as recommended by the manufacturer. The blots were washed finally in 0.1 × SSC/0.1% SDS at 55°C and exposed to X-ray film at − 80°C. For RT–PCR, cDNA was synthesized using the ThermoScript RT–PCR system (Life Technologies, Grand Island, NY).

Light microscopy and immunohistochemistry

PAS and immunohistochemical stainings were done as described previously (36). Sections were reacted with biotinylated IgM monoclonal mouse antibody KM279 and visualized using peroxidase-labeled streptavidin conjugate (Dako, Copenhagen). For double labeling, sections were reacted simultaneously with mouse monoclonal KM279 and rabbit polyclonal anti-ubiquitin antibodies (Dako), followed by anti-mouse IgG–rodamine and anti-rabbit IgG–FITC conjugates, and the fluorescence was observed by a confocal laser scanning microscope. The monoclonal anti-AGEP IgG was obtained commercially (TransGenic Inc., Kumamoto, Japan). TUNEL was performed on paraffin sections using the DeadEND Colorimetric Apoptosis Detection System as described by the manufacturer (Promega corporation, Madison, WI).

Electron microscopy

Different age groups of mice were perfused intracardially through the left ventricle with an ice-cold solution of 4% paraformaldehyde and 2.5% glutaraldehyde in 0.1 M phosphate buffer, pH 7.4. The perfusions were followed by a 24-hour immersion fixation at 4°C in the same solution. Tissue samples were harvested, embedded in both cross and longitudinal orientations, and processed for electron microscopic analyses.

Startle response test

In the acoustic startle test, mice were exposed to 40 ms broadband 110 dB burst (pulse trials) with an intertrial interval of 20 s (TIK Co. Ltd, Tokyo). Forty pulse trials were administered in total. The startle response was recorded for 1 s starting with the onset of the startle stimulus.

Step-through passive avoidance test

During the acquisition trial, animals were placed in the non-preferred bright chamber of a two-chamber apparatus (Ohara Co. Ltd, Tokyo, Japan). When animals entered the dark side, the door between the chambers was shut and the animal received a 0.4 mA, 5 s shock. After 10 s, the mice were returned to their home cage. Mice were tested 24 hours after the training, and the latency to enter to the dark chamber during the retention trial was recorded.

Rotarod test

A 3 cm diameter rotarod (Rota-Rod treadmill; Ugo Basile, Comerio, Italy) consisting of a plastic roller flanked by two round plastic plates was used for testing neuromuscular abnormalities. Mice were placed on a stationary cylinder. After 3 s, the rotarod was switched on, rotating evenly at a speed of 20 r.p.m. The ability of the mice to stay on the rotarod was timed until they fell, with a maximum cutoff of 200 s. Mice were tested for three trials on succeeding days, and the fourth trial was done on day 6, after a 2-day rest.

Hanging wire test

The ability to hang upside-down from a wire screen was tested as described previously (37). After naive mice were placed on a modified wire cover to a rat tub cage, the cover was waved gently for three times and immediately turned upside down. Latency to time of falling from the cover was recorded. Mice that fell within 10 s were given a second trial and those that did not fall during the 60 s trial period were removed and given a maximum score of 60 s.

Test for muscle strength

Grip strength of the forepaws was assessed at the point when mice released a horizontal strain gauge grasped by both front paws as a result of gentle traction applied to the tail. The gauge was connected to a gram dynamometer (Ohba Siki, Tokyo) that measured the force exerted.

Myoclonic seizure activity

Groups of animals (30 for each genotype) were monitored by constant videotaping using an automated seizure detection system (COBAS; GE Marquette Medical System, Kyoto) (17) for three consecutive days. Occurrence and frequency of myoclonic jerks were scored for each animal during dark and light periods separately.

EEG and ECoG recordings

Brain waves were recorded in two ways. (i) Electroencephalography (EEG): ten null mutant mice and accompanying heterozygous and wild-type littermates received 10–20 mg/kg of intraperitoneal sodium pentobarbital to induce stage 1 and 2 sleep. The scalp EEG was then recorded for 60–120 minutes using subdermal needle electrodes and a Caldwell digitized EEG. (ii) Electrocorticography (ECoG): six null mutants and four wild-type littermates were used for the EcoG recording. Under sodium pentobarbital anesthesia (40 mg/kg) five stainless screw electrodes (0.95 mm in diameter), directed toward and over frontal and occipital cortices of both cerebral hemispheres, were implanted in the skull. After a recovery period of 7 days, ECoG was recorded using amplifiers and MacLab system. Cortical recording was made on awake animals freely moving in the test box for a period of 20 minutes.

ACKNOWLEDGEMENTS

We thank K. Shoda, N. Nishiyama, Y. Onodera, C. Uchikawa, A. Rondan, F. Pasos, J. Espinosa and P. Aley for technical support, and M. Hooper for the E14 ES cell line. This study was supported in part by a grant from CURE (Citizens United for Research in Epilepsy) and the Lafora Disease associations of Sweden (Vera Faludi) and Quebec (Audette Malenfant) to A.V.D.-E.

REFERENCES

1. Lafora, G.R. and Glueck, B. (1911) Contribution to the histopathology and pathogenesis of myoclonic epilepsy. Bull. Gov. Hosp. Insane, 3, 96–111.
2. Schwarz, G.A. (1977) Lafora's disease: a disorder of carbohydrate metabolism. In Goldensohn, E.S. and Appel, S.H (eds), Scientific Approaches to Clinical Neurology. Lea & Febiger, Philadelphia, pp. 148–159.
3. Van Heycop Ten Ham, M.W. (1975) Lafora disease, a form of progressive myoclonus epilepsy. In Vinken, P.J. and Bruyn, G.W (eds), The Epilepsies. Handbook of Clinical Neurology 15, North-Holland, Amsterdam, pp. 382–422.
4. Serratosa, J.M., Delgado-Escueta, A.V., Posada, I., Shih, S., Drury, I., Berciano, J., Zabala, J.A., Antunez, M.C. and Sparkes, R.S. (1995) The gene for progressive myoclonus epilepsy of the Lafora type maps to chromosome 6q. Hum. Mol. Genet., 4, 1657–1663.
5. Acharya, J.N., Satischandra, P., Asha, T. and Shankar, S.K. (1993) Lafora's disease in South India: a clinical, electrophysiologic, and pathologic study. Epilepsia, 34, 476–487.
6. Delgado-Escueta, A.V., Ganesh, S. and Yamakawa, K. (2001) Advances in the genetics of progressive myoclonus epilepsy. Am. J. Med. Genet., 106, 129–138.
7. Minassian, B.A., Lee, J.R., Herbrick, J.A., Huizenga, J., Soder, S., Mungall, A.J., Dunham, I., Gardner, R., Fong, C.Y., Carpenter, S. et al. (1998) Mutations in a gene encoding a novel protein tyrosine phosphatase cause progressive myoclonus epilepsy. Nat. Genet., 20, 171–174.
8. Serratosa, J.M., Gomez-Garre, P., Gallardo, M.E., Anta, B., de Bernabe, D.B., Lindhout, D., Augustijn, P.B., Tassinari, C.A., Malafosse, R.M., Topcu, M. et al. (1999) A novel protein tyrosine phosphatase gene is mutated in progressive myoclonus epilepsy of the Lafora type (EPM2). Hum. Mol. Genet., 8, 345–352.
9. Ganesh, S., Agarwala, K.L., Ueda, K., Akagi, T., Shoda, K., Usui, T., Hashikawa, T., Osada, H., Delgado-Escueta, A.V. and Yamakawa, K. (2000) Laforin, defective in the progressive myoclonus epilepsy of Lafora type, is a dual-specificity phosphatase associated with polyribosomes. Hum. Mol. Genet., 9, 2251–2261.
10. Ganesh, S., Amano K. Delgado-Escueta, A.V. and Yamakawa, K. (1999) Isolation and characterization of mouse homologue for the human epilepsy gene, EPM2A. Biochem. Biophys. Res. Commun., 257, 24–28.
11. Ganesh, S., Agarwala, K.L., Amano, K., Suzuki, T., Delgado-Escueta, A.V. and Yamakawa, K. (2001) Regional and developmental expression of Epm2a gene and its evolutionary conservation. Biochem. Biophys. Res. Commun., 283, 1046–1053.
12. Busard, H.L.S.M., Renier, W.O, Gabreels, F.J.M., Jasper, H.H.J., Slooff, J.L., Janssen, A.J.M. and van Haelst, U.J.G. (1987) Lafora disease: a quantitative morphological and biochemical study of the cerebral cortex. Clin. Neuropathol., 6, 1–6.
13. Yokota, T., Ishihara, T., Yoshida, H., Takahashi, M., Uchino, F. and Hamanaka, S. (1988) Monoclonal antibody against polyglucosan isolated

from the myocardium of a patient with Lafora disease. J. Neuropathol. Exp. Neurol., 47, 572–577.
14. Monnier, V.M. and Cerami, A. (1981) Nonenzymatic browning in vivo: possible process for aging of long-lived proteins. Science, 211, 491–493.
15. Horiuchi, S., Araki, N. and Morino, Y. (1991) Immunochemical approach to characterize advanced glycation end products of the Maillard reaction. Evidence for the presence of a common structure. J. Biol. Chem., 266, 7329–7332.
16. Araki, N., Ueno, N., Chakrabarti, B., Morino, Y. and Horiuchi, S. (1992) Immunochemical evidence for the presence of advanced glycation end products in human lens proteins and its positive correlation with aging. J. Biol. Chem., 267, 10211–10214.
17. Amano, S., Yokoyama, M., Torii, R., Fukuoka, J., Tanaka, K., Ihara, N. and Hazama, F. (1997) High performance seizure-monitoring system using a vibration sensor and videotape recording: behavioral analysis of genetically epileptic rats. Lab. Anim. Sci., 47, 317–320.
18. Turmaine, M., Raza, A., Mahal, A., Mangiarini, L., Bates, G.P. and Davies, S.W. (2000) Nonapoptotic neurodegeneration in a transgenic mouse model of Huntington's disease. Proc. Natl Acad. Sci. USA, 97, 8093–8097.
19. Yokoi, S. and Austin, J. (1968) Studies in myoclonus epilepsy (Lafora body form). Arch. Neurol., 19, 15–33.
20. Yokoi, S., Nakayama, H. and Negishi, T. (1975) Biochemical studies on tissues from a patient with Lafora disease. Clin. Chim. Acta, 62, 415–423.
21. Wang, J., Stuckey, J.A., Wishart, M.J., and Dixon, J.E. (2002) A unique carbohydrate binding domain targets the Lafora disease phosphatase to glycogen. J. Biol. Chem., 277, 2377–2380.
22. Raben, N., Danon, M., Lu, N., Lee, E., Shliselfeld, L., Skurat, A.V., Roach, P.J., Lawrence, J.C. Jr., Musumeci, O., Shanske, S., DiMauro, S., Plotz, P. (2001) Surprises of genetic engineering: a possible model of polyglucosan body disease. Neurology, 56, 1739–1745.
23. Cavanagh, J.B. (1999) Corpora-amylacea and the family of polyglucosan diseases. Brain Res. Rev., 29, 265–295.
24. Lowe, J., Mayer, R.J. and Landon, M. (1993) Ubiquitin in neurodegenerative disease. Brain Pathol., 3, 55–65.
25. Smith, M.A., Taneda, S., Richey, P.L., Miyata, S., Yan, S.D., Stern, D., Sayre, L.M., Monnier, V.M. and Perry, G. (1994) Advanced Maillard reaction end products are associated with Alzheimer disease pathology. Proc. Natl Acad. Sci. USA, 91, 5710–5714.
26. Castellani, R., Smith, M.A., Richey, P.L. and Perry, G. (1996) Glycoxidation and oxidative stress in Parkinson disease and diffuse Lewy body disease. Brain Res., 737, 195–200.
27. Alves-Rodrigues, A., Gregori, L. and Figueiredo-Pereira, M.E. (1998) Ubiquitin, cellular inclusions and their role in neurodegeneration. Trends Neurosci., 21, 516–520.
28. Much, G., Cunningham, A.M., Riederer, P. and Braak, E. (1998) Advanced glycation end products are associated with Hirono bodies in Alzheimer's disease. Brain Res., 796, 307–310.
29. Shibata, N., Hirano, A., Kato, S., Nagai, R., Horiuchi, S., Komori, T., Umahara, T., Asayama, K. and Kobayashi, M. (1999) Advanced glycation endproducts are deposited in neuronal hyaline inclusions: a study on familial amyotrophic lateral sclerosis with superoxide dismutase-1 mutation. Acta Neuropathol. (Berl.), 97, 240–246.
30. Zoghbi, H.Y and Orr, H.T. (2000) Glutamine repeats and neurodegeneration. Annu. Rev. Neurosci., 23, 217–247.
31. Bence, N.F., Sampat, R.M. and Kopito, R.R. (2001) Impairment of the ubiquitin-proteasome system by protein aggregation. Science, 292, 1552–1555.
32. Yan, S.D., Schmidt, A.M., Anderson, G.M., Zhang, J., Brett, J., Zou, Y.S., Pinsky, D. and Stern, D. (1994) Enhanced cellular oxidant stress by the interaction of advanced glycation end products with their receptors/binding proteins. J. Biol. Chem., 269, 9889–9897.
33. Smith, M.A., Sayre, L.M., Monnier, V.M. and Perry, G. (1995) Radical AGEing in Alzheimer's disease. Trends Neurosci., 18, 172–176.
34. Yan, S.D., Chen, X., Fu, J., Chen, M., Zhu, H., Roher, A., Slattery, T., Zhao, L., Nagashima, M., Morser, J. et al. (1996) RAGE and amyloid-beta peptide neurotoxicity in Alzheimer's disease. Nature, 382, 685–691.
35. Schmidt, A.M., Yan, S.D., Yan, S.F. and Stern, D.M. (2000) The biology of the receptor for advanced glycation end products and its ligands. Biochim. Biophys. Acta, 1498, 99–111.
36. Mitsuno, S., Takahashi, M., Gondo, T., Hoshii, Y., Hanai, N., Ishihara, T. and Yamada, M. (1999) Immunohistochemical, conventional and immunoelectron microscopical characteristics of periodic acid–Schiff-positive granules in the mouse brain. Acta. Neuropathol. (Berl.), 98, 31–38.
37. Sango, K., McDonald, M.P., Crawley, J.N., Mack, M.L., Tifft, C.J., Skop, E., Starr, C.M., Hoffmann, A., Sandhoff, K., Suzuki, K. et al. (1996) Mice lacking both subunits of lysosomal beta-hexosaminidase display gangliosidosis and mucopolysaccharidosis. Nat. Genet., 14, 348–352.